ADVANCED FUNCTIONAL MATERIALS
www.afm-journal.de

Engineering Solar Cell Absorbers by Exploring the Band Alignment and Defect Disparity: The Case of Cu- and Ag-Based Kesterite Compounds

Zhen-Kun Yuan, Shiyou Chen, Hongjun Xiang, Xin-Gao Gong, Aron Walsh, Ji-Sang Park, Ingrid Repins, and Su-Huai Wei*

The development of kesterite $Cu_2ZnSn(S,Se)_4$ thin-film solar cells is currently hindered by the large deficit of open-circuit voltage (V_{oc}), which results from the easy formation of Cu_{Zn} antisite acceptor defects. Suppressing the formation of Cu_{Zn} defects, especially near the absorber/buffer interface, is thus critical for the further improvement of kesterite solar cells. In this paper, it is shown that there is a large disparity between the defects in Cu- and Ag-based kesterite semiconductors, i.e., the Cu_{Zn} or Cu_{Cd} acceptor defects have high concentration and are the dominant defects in $Cu_2ZnSn(S,Se)_4$ or Cu_2CdSnS_4, but the Ag_{Zn} acceptor has only a low concentration and the dominant defects are donors in Ag_2ZnSnS_4. Therefore, the Cu-based kesterites always show p-type conductivity, while the Ag-based kesterites show either intrinsic or weak n-type conductivity. Based on this defect disparity and calculated band alignment, it is proposed that the V_{oc} limit of the kesterite solar cells can be overcome by alloying $Cu_2ZnSn(S,Se)_4$ with $Ag_2ZnSn(S,Se)_4$, and the composition-graded $(Cu,Ag)_2ZnSn(S,Se)_4$ alloys should be ideal light-absorber materials for achieving higher efficiency kesterite solar cells.

1. Introduction

As the leading thin-film solar cell technology, CdTe and $Cu(In,Ga)Se_2$ (CIGS) solar cells have advanced to reach light-to-electricity conversion efficiencies over 20%, with annual production now in the gigawatt range.[1] However, as this volume increases, the cost and scarcity of In and Te, as well as the toxicity of Cd, could become major issues that may limit the widespread utilization of CdTe and CIGS photovoltaics. Therefore, the search and optimization of alternative thin-film solar cell materials is urgently needed. Quaternary I_2–II–IV–VI_4 (I = Cu, Ag, II = Zn, Cd, IV = Si, Ge, Sn, VI = S, Se, Te)[2] chalcogenides form a large group of semiconductors with variable structural, optical, and electrical properties.[3–7] Among them, the kesterite semiconductors Cu_2ZnSnS_4 and $Cu_2ZnSnSe_4$ have recently emerged as promising light-absorber materials for thin-film solar cells because of their close-to-optimal material properties.[8–13] Furthermore, all their component elements are earth-abundant and nontoxic, so they are expected to be ideal substitute for the currently commercialized CdTe and CIGS absorbers.

Despite their good material properties such as suitable band gap and high optical absorption, the increased number of elements in the quaternary compounds also results in a large amount of native lattice defects.[14–20] In Cu_2ZnSnS_4 (similarly $Cu_2ZnSnSe_4$), it was found that the Cu_{Zn} antisite defects have a low formation energy and high concentration due to the small size and chemical difference between Cu and Zn,[15,19] making the synthesized samples always show p-type conductivity.[21–25] When forming a p–n junction with the n-type CdS (buffer layer), the p-type Cu_2ZnSnS_4 (absorber layer) cannot have an effective p-to-n type inversion near the p–n junction interface because high concentration of Cu_{Zn} will form at the interface and pin the Fermi level at the middle of the band gap.[15] Experimentally it was found that the surface of Cu_2ZnSnS_4 is indeed p-type (without type inversion),[26] in agreement with the theoretical analysis. As a result, only a small band bending can be induced in the absorber layer, as shown in **Figure 1**a. Since the maximum V_{oc} of the solar cell

Z.-K. Yuan, Prof. H. Xiang, Prof. X.-G. Gong
Key Laboratory for Computational Physical Sciences (MOE)
State Key Laboratory of Surface Physics and Department of Physics
Collaborative Innovation Center of Advanced Microstructures
Fudan University
Shanghai 200433, China
Prof. S. Chen
Key Laboratory of Polar Materials and Devices (MOE)
East China Normal University
Shanghai 200241, China
E-mail: chensy@ee.ecnu.edu.cn
Prof. A. Walsh
Center for Sustainable Chemical Technologies and Department of Chemistry
University of Bath
Bath BA2 7AY, UK
Dr. J.-S. Park, Dr. I. Repins, Dr. S.-H. Wei
National Renewable Energy Laboratory
Golden, CO 80401, USA

DOI: 10.1002/adfm.201502272

© 2015 WILEY-VCH Verlag GmbH & Co. KGaA, Weinheim

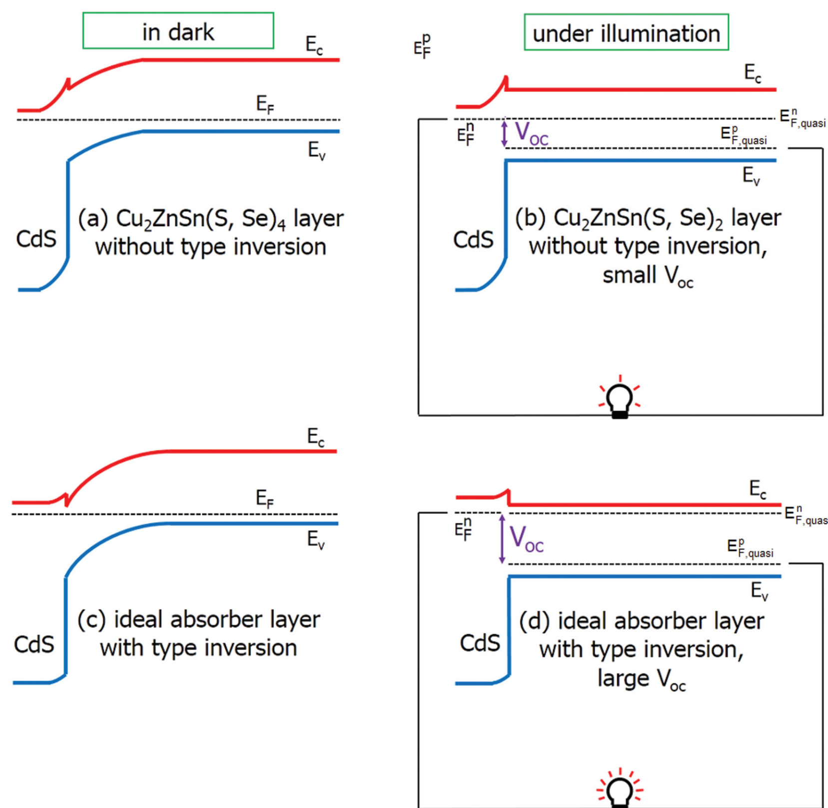

Figure 1. The band diagram of solar cells in the dark (left) and under illumination (right): a) the CdS/$Cu_2ZnSn(S,Se)_4$ solar cell with no type inversion (the Fermi level near the interface is pinned at the middle of the band gap) and small band bending in the absorber layer, b) the CdS/$Cu_2ZnSn(S,Se)_4$ solar cell with a small V_{oc} under the flat band condition, c) an ideal absorber layer with type inversion (the Fermi level near the interface is close to the conduction band) and a large band bending, and d) an ideal absorber layer with a large V_{oc} under the flat band condition. The band bending in the n-type CdS layer is not changed much under illumination because its absorption of visible light is weak and the concentration of the majority of electron carriers is not changed significantly by the photogenerated carriers. As we can see, the maximum V_{oc} under illumination is derived mostly from the band bending of the absorber layer in the dark.[27–29]

under illumination (under the flat band condition, as shown in Figure 1b) is equal to the band bending of the absorber layer in dark,[27–29] the Fermi level pinning by Cu_{Zn} defects (thus no type inversion) causes a large deficit of V_{oc}. This intrinsic defect problem has hindered the further progress of Cu-based kesterite solar cells, the record efficiency is only 12.7%,[30] still much lower than those of the CdTe and CIGS cells despite they have similar band gaps. In contrast, the type inversion (through forming n-type Cu-poor ordered vacancy compounds or Cd_{Cu} doping near the CdS/CIGS interface) and thus a large band bending have been observed in CIGS solar cells,[28,31–35] which makes their maximum V_{oc} much higher than that of the $Cu_2ZnSn(S,Se)_4$ solar cells, as shown in Figure 1c,d. It is thus critical to suppress the formation of Cu_{Zn} and make the type inversion possible at the p–n junction interface if one intends to overcome the V_{oc} deficit of $Cu_2ZnSn(S,Se)_4$ solar cells.

The detrimental effect of the acceptor defect Cu_{Zn} is further amplified because it can bind with donor defects such as Zn_{Cu} and Sn_{Zn}, forming high concentration of Cu_{Zn}+Zn_{Cu}, Cu_{Zn}+Sn_{Zn}, and $2Cu_{Zn}$+Sn_{Zn} defect complexes, which can cause band gap and electrostatic potential fluctuations[36–43] and/or the trapping and recombination of the carriers, thus further limiting the V_{oc}.[30,37,44–47] To suppress the Cu_{Zn} related defects, Cu-poor/Zn-rich growth conditions are required to fabricate high-efficiency Cu_2ZnSnS_4-based solar cells.[48–52] Unfortunately, this approach can cause the formation of secondary phases such as ZnS, too high concentrations of Cu vacancies, and serious nonstoichiometry, which can also limit device performance.[51,53–60] Therefore, how to suppress the formation of Cu_{Zn} and related defects imposes a great challenge to the further optimization of kesterite solar cells.

One of the possible approaches to suppress the formation of Cu_{Zn} is to substitute Cu or Zn in Cu_2ZnSnS_4 or $Cu_2ZnSnSe_4$ by atoms with different sizes, e.g., replacing Zn by Cd to form Cu_2CdSnS_4 or replacing Cu by Ag to form Ag_2ZnSnS_4. Considering the large size mismatch between Cu and Cd (Ag and Zn), we expect that Cu_{Cd} in Cu_2CdSnS_4 (Ag_{Zn} in Ag_2ZnSnS_4) may have high formation energy, then these two semiconductors may have significantly different defect properties from that in Cu_2ZnSnS_4 and thus the potential to overcome the V_{oc} bottleneck. Although this approach is in principle simple, whether it is efficient is still a question. Previous experiments have shown that undoped Ag_2ZnSnS_4 exhibits intrinsic n-type conductivity,[61,62] however, Cu_2CdSnS_4 retains p-type conductivity,[63–65] similar to that of Cu_2ZnSnS_4. This is not fully in accordance with our expectation. Why the Cu_2CdSnS_4 samples are p-type while Ag_2ZnSnS_4 samples are n-type, and what defects are dominant in determining their electrical conductivity? These questions are still open. A systematical study on the defects in these semiconductors is necessary for answering these questions and will also reveal whether the V_{oc} limit can be overcome by the element-substitution approach. One recent study showed that the efficiency of Cu_2ZnSnS_4 solar cell can be enhanced significantly from 5.30% to 9.24% through forming $Cu_2Zn_{1-x}Cd_xSnS_4$ alloys as the absorber layer,[66] showing that the replacement of Zn by Cd may have great potential for improving the device performance.

In this article, we have systematically investigated the intrinsic defects of Cu_2CdSnS_4 and Ag_2ZnSnS_4 based on the density functional theory calculations and compared them with those of Cu_2ZnSnS_4. Interestingly, we find that the Cu_{Cd} antisite related defects still have high concentration in Cu_2CdSnS_4 (similar to the case in Cu_2ZnSnS_4), making the samples intrinsically p-type. In contrast, the formation of Ag_{Zn} antisite defects is suppressed in Ag_2ZnSnS_4 with a lower equilibrium concentration

© 2015 WILEY-VCH Verlag GmbH & Co. KGaA, Weinheim

than three donor defects (Zn_{Ag}, Sn_{Zn} antisites and S vacancies). All the intrinsic point defects in Ag_2ZnSnS_4 have relatively high formation energy, so the samples show either poor or weak n-type conductivity. Based on the calculated valence band alignment, we explain the puzzling disparity in the defect properties of Cu- and Ag-based I_2–II–IV–VI_4 semiconductors, i.e., antisite defect formation is not solely determined by the size difference of the elements; the easy formation of Cu_{Zn} and Cu_{Cd} antisites in Cu-based compounds also results from the high valence band energy, determined by the Cu 3d level, while the suppressed formation of Ag_{Zn} in the Ag-based compounds results from the lower valence band edge determined by Ag 4d. Our results reveal a fundamental distinction between the defect physics of the Cu- and Ag-based I_2–II–IV–VI_4 semiconductors, based on which and calculated band alignment between Cu- and Ag-based kesterites, we propose that forming composition- and band-graded $(Cu_{1-x}Ag_x)_2ZnSn(S,Se)_4$ alloy absorber should have great potential to overcome the V_{oc} deficit and improve the solar cell efficiency.

2. Results and Discussion

2.1. Defect Similarity between Cu-Based Cu_2CdSnS_4 and Cu_2ZnSnS_4

Since the size difference between Cu and Cd is large (the calculated Cu—S and Cd—S bond lengths in Cu_2CdSnS_4 are 2.32 and 2.56 Å, as shown in **Table 1**), we expected that the formation energy of the Cu_{Cd} antisite may be high and the dominant defect will be the shallow Cu vacancy V_{Cu}, similar to that in the ternary $CuInSe_2$ and $CuGaSe_2$.[67,68] Surprisingly, our first-principles formation energies show a different picture. The Cu_{Cd} antisite defect still has a low formation energy, slightly higher than Cu_{Zn} in Cu_2ZnSnS_4 by about 0.2 eV, indicating that the formation energies of Cu_{Cd} and Cu_{Zn} antisite (more generally I_{II} in I_2-II-IV-VI_4) may not be determined just by the size difference, in contrast to intuition. Cu_{Cd} is still the lowest-energy acceptor defect in Cu_2CdSnS_4, no matter what chemical potential conditions are considered, as shown in **Figure 2**. V_{Cu} has much higher formation energy (0.8–1.3 eV) than Cu_{Cd} (0.3–0.6 eV), and all other acceptor and donor defects have higher formation

Table 1. Calculated bond length and defect formation energy of neutral V_I and I_{II} defects in Cu_2ZnSnS_4, Cu_2CdSnS_4, and Ag_2ZnSnS_4. Both the value when $\mu_{Cu} = \mu_{Cd} = \mu_{Zn} = \mu_{Ag} = 0$ and the largest value in the achievable chemical potential region are shown for comparison.

	Bond length [Å]		Formation energy [eV]			
			$\mu_{Cu} = \mu_{Cd} = \mu_{Zn} = \mu_{Ag} = 0$		Maximum	
Cu_2ZnSnS_4	Cu—S	2.31	V_{Cu}	1.14[15]	V_{Cu}	1.14[15]
	Zn—S	2.36	Cu_{Zn}	1.41	Cu_{Zn}	0.38[15]
Cu_2CdSnS_4	Cu—S	2.32	V_{Cu}	1.28	V_{Cu}	1.28
	Cd—S	2.56	Cu_{Cd}	1.28	Cu_{Cd}	0.59
Ag_2ZnSnS_4	Ag—S	2.57	V_{Ag}	2.14	V_{Ag}	2.14
	Zn—S	2.36	Ag_{Zn}	3.10	Ag_{Zn}	1.80

energies in their neutral charge state, so the dominance of the acceptor Cu_{Cd} makes Cu_2CdSnS_4 show intrinsic p-type conductivity, similar to that in Cu_2ZnSnS_4 where Cu_{Zn} is the dominant defect.[15]

If we compare the formation energy when $\mu_{Cu} = \mu_{Cd} = 0$, the value of Cu_{Cd} (1.28 eV) is actually equal to that of V_{Cu}. However, μ_{Cd} is rather low, always lower than –0.9 eV because of the easy formation of the binary CdS (as shown in Figure S1 of the Supporting Information), which decreases the formation energy of Cu_{Cd} according to Equation (1) and changes the energy order of Cu_{Cd} and V_{Cu}. Therefore, the constraint on the Cd chemical potential by CdS plays an important role in the dominance of Cu_{Cd} antisite.

The low formation energy of Cu_{Cd} makes n-type doping of Cu_2CdSnS_4 difficult because when the Fermi level increases, the ionized Cu_{Cd} acceptor defect can reduce its formation energy to zero (see Figure 2a), thus forming spontaneously and limiting the further increase of the Fermi level. In the kesterite solar cells, there is a p–n heterojunction between the p-type absorber layer (Cu_2ZnSnS_4 or Cu_2CdSnS_4) and the n-type buffer layer (CdS). As shown in Figure 1, a p-to-n type inversion of the absorber layer is required near the junction interface so that a large band bending (as large as the band gap) can be formed from the interior of the absorber layer to the junction interface. This band bending determines the open-circuit voltage (V_{oc}) of the solar cell. Because of the n-type doping difficulty (the Fermi level is pinned at the middle of the band gap), the type inversion cannot be effectively achieved under equilibrium in Cu_2ZnSnS_4 or Cu_2CdSnS_4, so the band bending is small and the V_{oc} is severely limited to a small value, as shown in Figure 1b.

Furthermore, as a result of the low formation energy of Cu_{Cd}, defect complexes based on Cu_{Cd}, such as the self-compensated antisite pair Cu_{Cd}+Cd_{Cu}, also have very low formation energies. The value for Cu_{Cd}+Cd_{Cu} is only 0.21 eV/pair (see Figure 2b), very close to the Cu_{Zn}+Zn_{Cu} pair in Cu_2ZnSnS_4 (0.20 eV/pair),[15,19] indicating that the Cu/Cd cation disorder is also common in Cu_2CdSnS_4. The formation of Cu_{Cd}+Cd_{Cu} antisite pairs induces a small band gap shrinking (as shown in **Figure 3**b), which can cause band gap fluctuations in different area of the samples. Besides the Cu_{Cd}+Cd_{Cu} pair, the formation energy of $2Cu_{Cd}$+Sn_{Cd} is also low, about 0.43–0.65 eV, comparable with that of $2Cu_{Zn}$+Sn_{Zn} clusters in Cu_2ZnSnS_4.[15] The $2Cu_{Cd}$+Sn_{Cd} complexes induce more significant downshift of the conduction band and also the upshift of the valence band, so its high population causes more significant band gap fluctuation and also the trapping of the electron carriers, which also leads to V_{oc} deficit in devices.

Except for Cu_{Cd} and V_{Cu} related defects, other donor and acceptor defects have high formation energies when they are not ionized. The high concentration of Cu_{Cd} defects makes the samples p-type and shifts the Fermi level to close to the VBM, so the donor defects such as Cd_{Cu}^{+}, Sn_{Cd}^{2+}, and Sn_{Cu}^{3+} become ionized and decrease their formation energy to lower than 1.0 eV (according to Equation (1), and even to only 0.62, 0.55, and 0.88 eV at the Sn-rich, Cu-poor, and Cd-poor condition (point P in Figure S1, Supporting Information). This suggests that these ionized donor defects exist in p-type Cu_2CdSnS_4 samples. From the calculated transition energy levels as shown in Figure 3a,

© 2015 WILEY-VCH Verlag GmbH & Co. KGaA, Weinheim

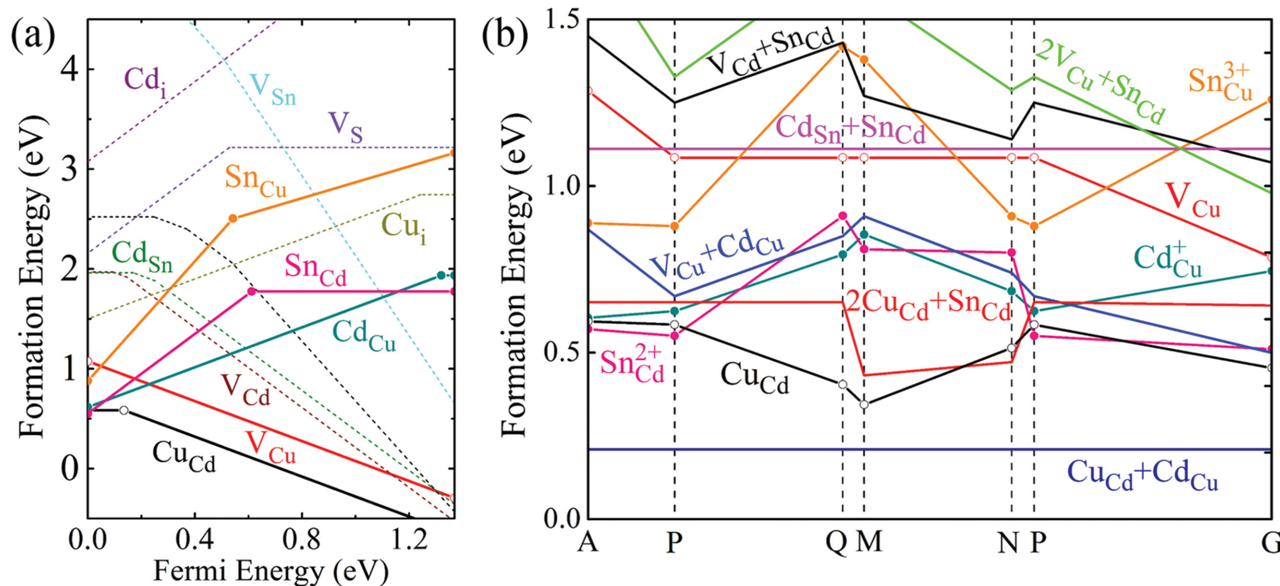

Figure 2. The calculated formation energy change of defects in Cu_2CdSnS_4 a) as a function of the Fermi level at the chemical potential point P and b) as a function of the elemental chemical potentials. The chemical potential points P–Q–M–N–G are shown in Figure S1 (Supporting Information), and $\mu_{Cu} = 0$, $\mu_{Cd} = -0.69$ eV, and $\mu_{Sn} = -0.29$ eV at the point A. The Fermi level is assumed to be at the VBM (p-type conditions), and therefore, all donor defects are ionized in panel (b).

the donor level of Cd_{Cu} is shallow, while those of Sn_{Cu} and Sn_{Cd} are deep in the gap and thus may act as electron-hole recombination centers. This is also similar to the deep-level donors Sn_{Cu} and Sn_{Zn} in Cu_2ZnSnS_4.[15] The calculated acceptor level of Cu_{Cd} is 0.13 eV above the valence band, relatively deeper than that of V_{Cu} (0.01 eV).

Given the relatively deep level of the dominant acceptor defect Cu_{Cd} as well as the existence of detrimental deep-level donor defects and defect complexes, the Cu_2CdSnS_4 solar cell performance should be limited. In order to suppress the formation of Cu_{Cd} and the detrimental donor defects and defect complexes, and also to increase the shallow acceptor V_{Cu}, Cu-poor, Sn-poor, but Cd-rich growth conditions are necessary. However, too Cd-rich condition also causes the existence of CdS, which should be avoided. Similar bottleneck effect exists also in Cu_2ZnSnS_4, where Zn-rich condition is required to suppress detrimental defects but it also causes the formation of ZnS secondary phase.[51,53–60]

Based on the above discussion, the main features of the defect properties of Cu_2CdSnS_4 and Cu_2ZnSnS_4 are very similar. Since the formation energies of deep-level donors are even lower in Cu_2CdSnS_4, we predict that the development of high-efficiency Cu_2CdSnS_4 solar cells is more challenging. Indeed, the achieved efficiency of Cu_2CdSnS_4-based solar cells is currently much lower than that of Cu_2ZnSnS_4-based solar cells.[64,69] After we finished the current work, we noticed a more recent study which shows that the solar cells based on $Cu_2Zn_{1-x}Cd_xSnS_4$ alloys with appropriate Zn/Cd ratio have an efficiency up to 9.24%, while the efficiency is decreased when the Cd content is high,[66] which can be understood according to our finding that high concentration of deep-level defects (recombination centers) exist in pure Cu_2CdSnS_4.

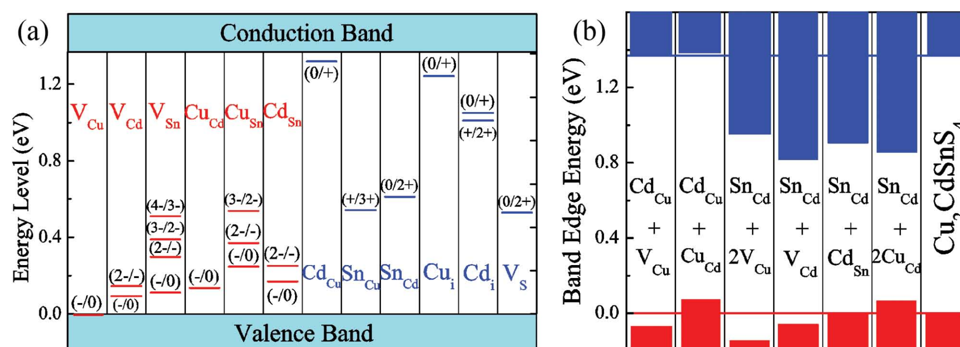

Figure 3. a) The transition energy levels of intrinsic point defects in the band gap of Cu_2CdSnS_4, and b) the band edge shift caused by the low-energy defect complexes. The GGA/DFT band gap is corrected to the experimental value of 1.38 eV. The band edge shift is calculated assuming one defect complex in a 64-atom supercell.

© 2015 WILEY-VCH Verlag GmbH & Co. KGaA, Weinheim

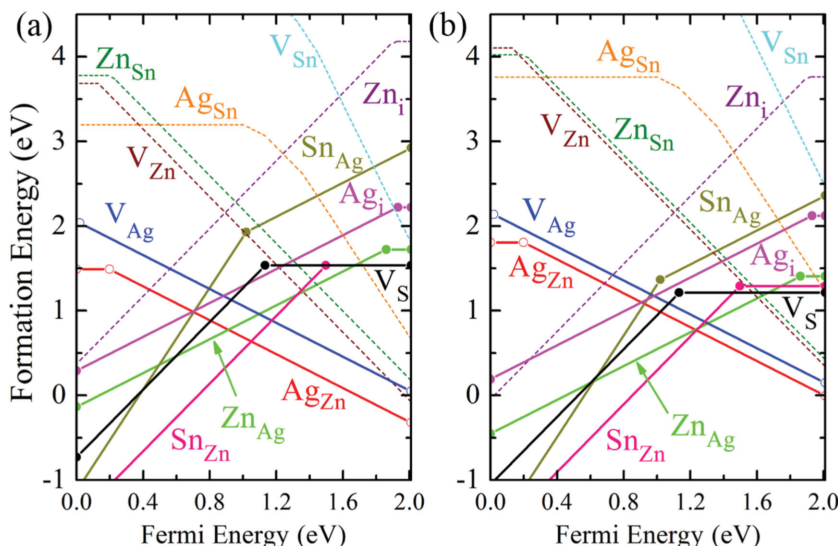

Figure 4. The calculated formation energy change as a function of the Fermi level for possible acceptor and donor defects in Ag_2ZnSnS_4. Two chemical potential points in Figure S1 (Supporting Information) a) M and b) P are considered. The slope shows the charge state of ionized defects (following Equation (1)), e.g., positive slope means ionized donor while negative slope means ionized acceptor defects. The GGA/DFT band gap is corrected to the experimental value of 2.01 eV.

2.2. Defect Disparity between Ag-Based Ag_2ZnSnS_4 and Cu-Based Cu_2ZnSnS_4

Unlike Cu_2CdSnS_4, we find the defect behavior of Ag_2ZnSnS_4 is remarkably different from that of Cu_2ZnSnS_4. As shown in **Figure 4**, the formation energy of Ag_{Zn} antisite increases to above 1.5 eV, much higher than that of Cu_{Zn} in Cu_2ZnSnS_4 and Cu_{Cd} in Cu_2CdSnS_4, in accordance with our expectation that the large difference between Ag and Zn may increase the formation energy of their antisite. When the chemical potentials of the elements are zero ($\mu_{Ag} = \mu_{Zn} = 0$), the formation energy of Ag_{Zn} is even larger, 3.10 eV, as shown in Table 1. Due to the competition from ZnS, the Zn chemical potential is limited to lower than −1.3 eV (shown in Figure S1 of the Supporting Information), which decreases the Ag_{Zn} formation energy by 1.3 eV. Comparing the formation energy of Ag_{Zn} in Ag_2ZnSnS_4, Cu_{Zn} in Cu_2ZnSnS_4, and Cu_{Cd} in Cu_2CdSnS_4 when the chemical potentials are zero (see Table 1), the value of Ag_{Zn} is much larger than that of Cu_{Zn} (1.41 eV) and Cu_{Cd} (1.28 eV). This cannot be fully explained by the size mismatch because the bond length difference between Ag—S and Zn—S is even smaller than that between Cu—S and Cd—S, but the formation energy of Ag_{Zn} is much larger than that of Cu_{Cd}. One possible reason is that it costs larger strain energy to replace one small cation (Zn) by one large cation (Ag) than replace one large cation (Cd) by one small cation (Cu), but this is not enough to explain the large energy difference around 1.2 eV between Ag_{Zn} and Cu_{Cd}. Therefore, other factors should play an important role in the high formation energy of Ag_{Zn} antisite, which will be discussed in Section 3.3.

Since the Ag_{Zn} antisite has a high formation energy, the formation of related defect complexes such as Ag_{Zn}+Zn_{Ag} and $2Ag_{Zn}$+Sn_{Zn} is also suppressed. Compared to the low formation energy (0.20 eV/pair) of Cu_{Zn}+Zn_{Cu} in Cu_2ZnSnS_4,[15,19] the formation energy of Ag_{Zn}+Zn_{Ag} is high (0.52 eV/pair), and that of $2Ag_{Zn}$+Sn_{Zn} is even higher (above 3 eV, so it is not shown in **Figure 5**). Other defect complexes including V_{Ag}+Zn_{Ag}, Zn_{Sn}+Sn_{Zn}, Ag_{Zn}+Ag_i, V_{Zn}+Sn_{Zn}, and $2V_{Ag}$+Sn_{Zn} have formation energies in the range 0.6–1.4 eV, showing that the existence of defect complexes is also possible in Ag_2ZnSnS_4, but their concentration and the influence (trapping of carriers) are much smaller than those in Cu_2ZnSnS_4.

The increase of Ag_{Zn} formation energy also changes the dominant defect in Ag_2ZnSnS_4. As shown in Figure 5, the acceptor Ag_{Zn} has the lowest formation energy among all the acceptor and donor defects only near the chemical potential point M, while the donor defects V_S, Sn_{Zn}, and Zn_{Ag} become the dominant defects at other chemical potential points. This can be seen more clearly in Figure 4, where the formation energy change of the neutral and ionized defects as a function of the Fermi level is plotted. At the chemical potential point M (Zn-poor, S-rich), the acceptor Ag_{Zn} has a formation energy slightly lower than those of the donors Sn_{Zn}, V_S, and Zn_{Ag} when they are charged neutral. When they are ionized, their competition will determine the Fermi level of the samples at around 1.0 eV, just in the middle of the band gap. Due to the compensation of the acceptor and donor defects, the carrier concentration of the samples will be low and thus the electrical conductivity will be very poor. At the chemical potential point P (Zn-rich, Sn-rich, and S-poor), the donor defects have lower formation energy than the acceptor ones, so the sample will show n-type conductivity. However, the formation of the acceptor Ag_{Zn} becomes spontaneous and compensates the electron carriers as the Fermi level approaches the conduction band (highly n-type), which limits the concentration of electron carriers. According to Figure 4b, we estimate that the Fermi level of the undoped Ag_2ZnSnS_4 samples is located at 0.8 eV below the CBM (the cross point of Zn_{Ag} and Ag_{Zn} lines) under equilibrium growth condition, so the conductivity is still poor despite the n-type character. At other chemical potential points such as A, the n-type conductivity increases slightly because the energy difference between the neutral Zn_{Ag} and Ag_{Zn} increases, but the increase is not large.

Considering all of the representative chemical potential points, we can predict that the electrical conductivity of undoped Ag_2ZnSnS_4 is always poor, i.e., either intrinsic or weakly n-type with low electron carrier concentration. This is dramatically different from the situation in Cu_2ZnSnS_4 and Cu_2CdSnS_4 where only p-type conductivity is possible and the n-type doping is impossible because of the spontaneous compensation of the acceptor defects (Cu_{Zn} and Cu_{Cd} antisites). Our prediction is in agreement with available experimental observations that i) only n-type Ag_2ZnSnS_4 samples have been synthesized and no p-type samples have been reported as far as

© 2015 WILEY-VCH Verlag GmbH & Co. KGaA, Weinheim

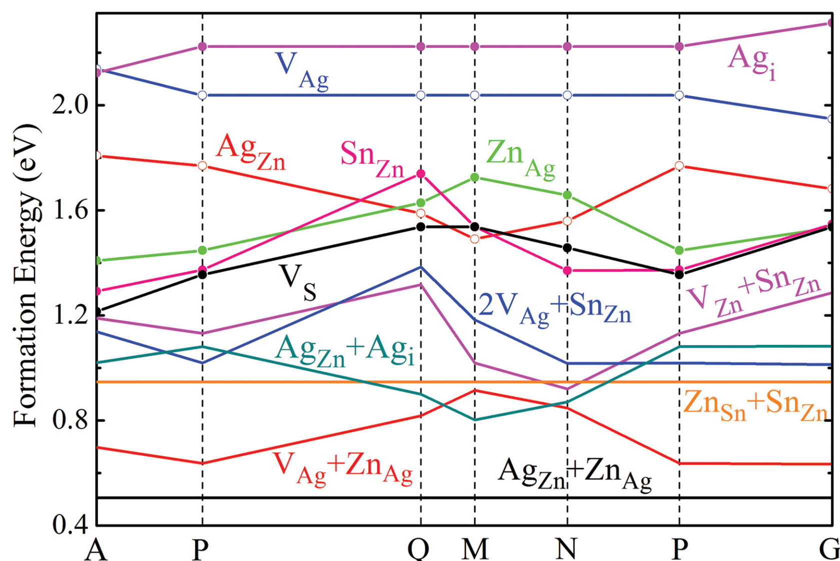

Figure 5. The calculated formation energy change as a function of the elemental chemical potentials (growth conditions) for low-energy defects and defect complexes in Ag_2ZnSnS_4. The chemical potential points P–Q–M–N–G are shown in Figure S1 (Supporting Information), and $\mu_{Ag} = 0$, $\mu_{Zn} = -1.30$ eV, and $\mu_{Sn} = -0.59$ eV at the point A.

we know,[61,70] and ii) the highest electron concentration measured so far is lower than 10^{14} cm^{-3} in Ag_2ZnSnS_4 samples.[61] This situation may be changed if suitable extrinsic dopants can be introduced. According to Figure 4, the formation energy of Ag_{Zn} decreases to zero only when the Fermi level is close to the CBM (the Fermi level is almost not pinned by Ag_{Zn}), so the Fermi level can be shifted up to close to the CBM if high concentration of extrinsic n-type dopants such as Cd_{Ag} can be introduced to the Ag_2ZnSnS_4 samples, then a high concentration of electron carriers and good n-type conductivity could be achieved.

In **Figure 6**, the calculated transition energy levels of defects are plotted. Ag_{Zn} has an acceptor level at 0.2 eV above the VBM, which is deeper than Cu_{Zn} and Cu_{Cd}. Among the low-energy donor defects, Zn_{Ag} has a relatively shallow level, so it plays an important role in determining the n-type conductivity. In contrast, both V_S and Sn_{Zn} have deep donor levels. Their ε (0/2+) transition levels are calculated at 0.88 and 0.51 eV below the conduction band, respectively. Therefore, their contribution to the n-type conductivity is small. Instead, their high concentration facilitates the recombination of electron and hole, which imposes a serious limitation on the application of Ag_2ZnSnS_4 as the photovoltaic and photocatalytic semiconductors.[71–73]

2.3. Influence of Band Edge Position on Defect Formation

As discussed above, the most important feature in the defect properties of Cu- and Ag-based I_2–II–IV–VI_4 semiconductors is that the Cu_{Cd} antisite related defects have low formation energy thus high concentration in Cu_2CdSnS_4, while the Ag_{Zn} antisite related defects have high formation energy thus low concentration in Ag_2ZnSnS_4. This is in contrast to our earlier expectation that the large size difference will suppress the formation of both Cu_{Cd} and Ag_{Zn}, indicating that there are other factors influencing the formation of the antisite defects.

One possible factor is the energy of the valence and conduction bands. **Figure 7**a shows the calculated band alignment of the Cu_2CdSnS_4, Cu_2ZnSnS_4, and Ag_2ZnSnS_4. The valence band edge of Ag_2ZnSnS_4 is lower (by 0.74 eV) than those of Cu_2CdSnS_4 and Cu_2ZnSnS_4. The low valence band edge position indicates that the binding energy of the valence electrons is high, and thus it will cost more energy to create a hole in (take an electron away from) the system. Because the formation of acceptor defects such as Cu_{Cd}, Cu_{Zn}, and Ag_{Zn} creates a hole near the valence band edge, the low valence band edge of Ag_2ZnSnS_4 increases the formation energy of Ag_{Zn}. The valence band edge positions of Cu_2CdSnS_4 and Cu_2ZnSnS_4 are comparably high, so the formation energies of Cu_{Cd} and Cu_{Zn} are both low, despite the fact that the size difference between Cu and Cd is much larger than between Cu and Zn. The influence of the band edge position exists not only for the antisite defects but also for other defects. For example, the Ag vacancy (V_{Ag}) in Ag_2ZnSnS_4 has a much higher formation energy than

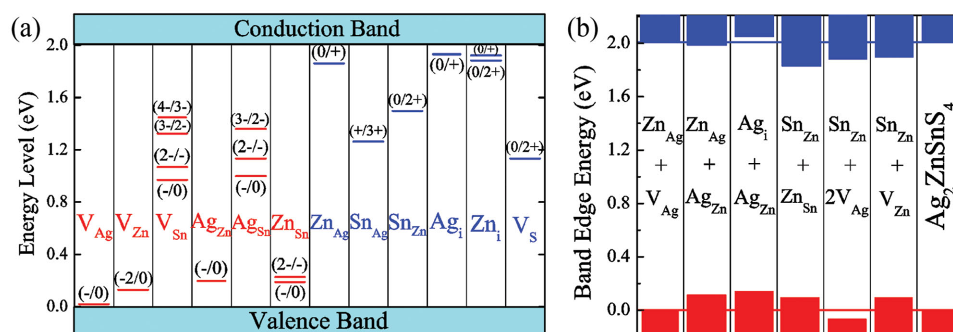

Figure 6. a) The transition energy levels of intrinsic point defects in the band gap of Ag_2ZnSnS_4 and b) the band edge shift caused by the low-energy defect complexes. The GGA/DFT gap is corrected to the experimental value of 2.01 eV. The band edge shift is calculated assuming one defect complex in a 64-atom supercell.

© 2015 WILEY-VCH Verlag GmbH & Co. KGaA, Weinheim

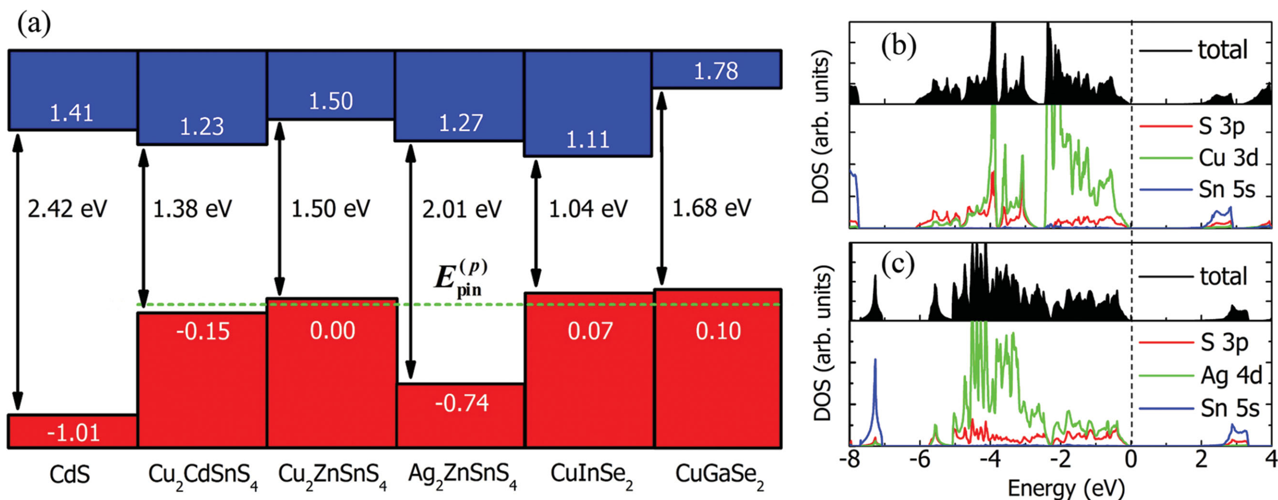

Figure 7. a) Calculated band alignment between Cu_2CdSnS_4, Cu_2ZnSnS_4, Ag_2ZnSnS_4, $CuInSe_2$, $CuGaSe_2$, and CdS; b,c) total and partial electronic density of states (DOS) of Cu_2CdSnS_4 and Ag_2ZnSnS_4. The calculation methods are described in ref. [74]. The dashed line shows the Fermi energy pinning level $E_{pin}^{(p)}$ for p-type doping.

Cu vacancy (V_{Cu}) in Cu_2CdSnS_4 and Cu_2ZnSnS_4, as shown in Figures 2 and 5.

It should be noted that the large formation energy of Ag_{Zn} is determined not only by the low valence band edge position. This can be seen clearly in the large formation energy difference (around 1.4 eV, see Figure 5 and Figure 7 of Chen et al.[15]) between Ag_{Zn} in Ag_2ZnSnS_4 and Cu_{Zn} in Cu_2ZnSnS_4, which is much larger than the difference of valence band edge positions (0.74 eV shown in Figure 7). Therefore, the larger formation energy of Ag_{Zn} is contributed not only by the lower valence band but also by the larger strain energy cost (estimated to be about 0.66 eV) caused by the larger size difference between Ag and Zn than that between Cu and Zn. Since the formation energy of Cu_{Cd} is just slightly (by about 0.2 eV) higher than Cu_{Zn}, and the difference is almost equal to the valence band offset between Cu_2CdSnS_4 and Cu_2ZnSnS_4 (0.15 eV), the strain energy cost in the formation of Cu_{Cd} should be small despite the large size difference between Cu and Cd. This can be understood considering that it costs smaller strain energy to replace one large cation (Cd) by one small cation (Cu) than replace one small cation (Zn) by one large cation (Ag). With the same argument, we can understand why the formation energy of the donor antisite defect Cd_{Cu} (large replaces small) is 0.6 eV larger than that of Zn_{Ag} (small replaces large) although their conduction band edge positions are comparable.

All the acceptor defects have high formation energies in Ag_2ZnSnS_4 due to the low valence band edge position, so the intrinsic defects cannot give rise to p-type conductivity. Furthermore, even if we intentionally introduce extrinsic dopants, the doping sites that produce acceptor levels will also have higher formation energies than the sites producing donor levels. Therefore, a p-type doping difficulty always exists for semiconductors such as Ag_2ZnSnS_4. This is known as the "doping limit rule."[67,75] A p-type doping limit level $E_{pin}^{(p)}$ (shown by the green dashed line in Figure 7) was proposed in the previous studies about the ternary chalcogenides $CuGaSe_2$ and $CuInSe_2$,[75–77] which have similar crystal and electronic structure to Cu_2CdSnS_4, Cu_2ZnSnS_4, and Ag_2ZnSnS_4. When the valence band edge is lower than this limit level, it is difficult to produce a high concentration of hole carriers and shift the Fermi level to below this level, no matter through the formation of intrinsic acceptor defects or doping of extrinsic elements.[34] The valence band edge of Ag_2ZnSnS_4 is about 0.7 eV lower than this level, so the high formation energy and low concentration of intrinsic acceptor defects (including Ag_{Zn}) in Ag_2ZnSnS_4 are consistent with this doping limit rule. The valence band edges of Cu_2CdSnS_4, Cu_2ZnSnS_4, $CuGaSe_2$, and $CuInSe_2$ are above or close to this level, so their Fermi level can be shifted to close to the valence band edge, i.e., high concentration of hole carriers (from ionized Cu_{Zn}, Cu_{Cd}, or V_{Cu}) and good p-type conductivity can be achieved in these semiconductors, in good agreement with the previous experimental observation.[21–25,63–65]

Since the band energy has direct influence on the defect formation, its control becomes important for tuning the defect and electrical properties of the semiconductors. To control the band edge positions, we need to know the component of the band edge states, which can be seen in the calculated partial and total density of states as shown in Figure 7. The top part of the valence bands of Cu_2CdSnS_4 (Ag_2ZnSnS_4) are composed of the hybridized states of the Cu 3d (Ag 4d) and S 3p orbitals, while the contribution from Zn and Sn orbitals is small, similar to the situation in Cu_2ZnSnS_4.[78,79] One obvious difference is that the high Ag 4d peaks are 4 eV below VBM, while the Cu 3d peaks are much higher, around 2 eV below the VBM. This results from the atomic energy level difference of Ag 4d and Cu 3d orbitals (the Ag 4d atomic levels are 2.3 eV lower than Cu 3d levels[5,85], so the hybridized states of the Ag 4d orbitals are lower in the valence band. The VBM consists of hybridized states of the Cu 3d (Ag 4d) and S 3p orbitals, so the lower Ag 4d atomic level also explains the lower valence band edge position of Ag_2ZnSnS_4. Furthermore, the Ag—S bond is longer than Cu—S bond, so the p–d hybridization is weaker between Ag and S than between Cu

© 2015 WILEY-VCH Verlag GmbH & Co. KGaA, Weinheim

and S, which also contributes to the lower valence band edge position of Ag_2ZnSnS_4.

According to this mechanism, the formation energies of the acceptor defects should also be high and thus the p-type doping should be difficult in other Ag—S or Ag—Se compounds with similar valence band component (Ag 4d and S 3p or Se 4p hybridized states). Interestingly, experiments showed that most of the synthesized Ag_2S, Ag_2Se, $AgInS_2$, $AgInSe_2$, and $Ag_2ZnSnSe_4$ samples show intrinsic n-type conductivity and their p-type doping is difficult,[81–90] in agreement with our prediction based on the atomic levels.

2.4. Strategy to Increase V_{oc} of Kesterite Solar Cells

Due to the significantly increased formation energy of Ag_{Zn} antisite, the V_{oc} bottleneck of Cu_2ZnSnS_4 solar cells caused by the spontaneous formation of Cu_{Zn} antisite defects at the interface (as mentioned in Section 1 and also shown schematically in **Figure 8**) can be largely avoided if it is replaced by Ag_2ZnSnS_4. However, since Ag_2ZnSnS_4 has poor electrical conductivity and defect levels are relatively deep, the solar cell performance should be limited if pure Ag_2ZnSnS_4 is used as the absorber layer.

Thus, one possible strategy to increase V_{oc} of Cu_2ZnSnS_4 solar cells is to form $(Cu_{1-x}Ag_x)_2ZnSnS_4$ alloys, in which the antisite acceptor defects are expected to have higher formation energy, so a large band bending can be achieved near the $(Cu_{1-x}Ag_x)_2ZnSnS_4$/CdS junction interface, and thus the V_{oc} can be increased. There exists an optimal value for the Ag composition parameter x because too high Ag composition can i) reduce the good p-type conductivity in the absorber region too much and even change it to n-type, ii) create more recombination center defects, and because iii) the band gap increases from the optimal value 1.5 eV to a larger one (2.01 eV when $x = 1$), causing the efficiency drop.

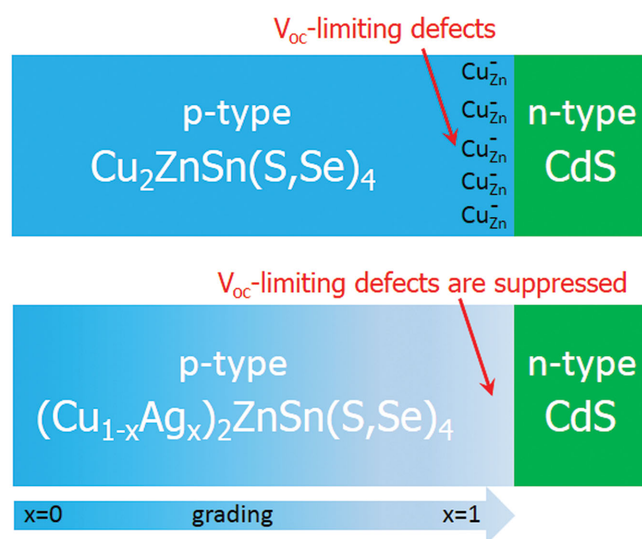

Figure 8. Schematic plot of the p–n junction interface between the n-type CdS buffer layer and p-type absorber layer: $Cu_2ZnSn(S,Se)_4$ with high concentration of Cu_{Zn} antisite defects limiting V_{oc} (top) and composition-graded $(Cu_{1-x}Ag_x)_2ZnSn(S,Se)_4$ free of V_{oc}-limiting defects (bottom). Note that Cu_{Zn} is everywhere inside the $Cu_2ZnSn(S,Se)_4$ absorber layer, however, its concentration is extremely high near the p–n junction interface because the Fermi level shifts up to a higher level (as shown in Figure 1a) and thus the formation energy of Cu_{Zn} decreases to a small value. When a high composition of Ag is alloyed into $(Cu_{1-x}Ag_x)_2ZnSn(S,Se)_4$ near the interface, the formation of Cu_{Zn} is suppressed.

Since high efficiency of the kesterite solar cells was usually based on the $Cu_2ZnSnSe_4$[8,91] or $Cu_2ZnSn(S,Se)_4$[9] alloys with high Se composition, we may apply the similar strategy to them, forming $(Cu_{1-x}Ag_x)_2ZnSnSe_4$ and $(Cu_{1-x}Ag_x)_2ZnSn(S,Se)_4$ alloys. According to the discussion in Section 3.3, the antisite acceptor defects also have high formation energies in the selenides, so the V_{oc} can be increased too. Furthermore, $Cu_2ZnSnSe_4$ has a small band gap of 1.0 eV while $Ag_2ZnSnSe_4$ has a larger gap, so the alloying will increase the band gap to closer to the optimal value, which makes the efficiency improvement more obvious in the alloys of the selenides than in the alloys of the sulfides.

Besides forming composition-uniform alloys, an even better choice to improve the V_{oc} and efficiency would be forming composition-graded $(Cu_{1-x}Ag_x)_2ZnSn(S,Se)_4$ alloys as the absorber layer with low Ag concentration in the back and higher Ag concentration in the region close to the $(Cu_{1-x}Ag_x)_2ZnSn(S,Se)_4$/CdS junction interface, as shown in Figure 8. This is because in the interior of the absorber layer good p-type conductivity and less recombination-center defects are needed, which can be achieved by pure $Cu_2ZnSn(S,Se)_4$ or $(Cu_{1-x}Ag_x)_2ZnSn(S,Se)_4$ alloy with low Ag concentration; however, close to absorber/buffer layer interface, suppressing the formation of Cu_{Zn} antisites is needed to make a p-to-n type inversion possible near the interface and thus to improve V_{oc}, which can be achieved by adding more and more Ag to the region when it is more and more close to the junction. In this way the negative effect of the Ag alloying is avoided, and meanwhile the type inversion becomes possible near the interface, which should improve the V_{oc} and the efficiency significantly, as shown in Figure 1. Moreover, there are two extra advantages: i) the higher band gap near the front can improve the light absorption and ii) the type-II band alignment between $Cu_2ZnSn(S,Se)_4$ and $Ag_2ZnSn(S,Se)_4$ (shown in Figure 7a for sulfides, where the CBM of Ag_2ZnSnS_4 is slightly lower than that of Cu_2ZnSnS_4, and the VBM of Ag_2ZnSnS_4 is significantly lower than that of Cu_2ZnSnS_4) makes both the valence and conduction bands have a downward slope from the back contact to the p–n junction interface, which can facilitate the electron-hole separation and thus reduce carrier recombination in this system. Therefore, a solar cell with composition-graded $(Cu_{1-x}Ag_x)_2ZnSn(S,Se)_4$ alloy as the absorber layer should have great potential to improve the V_{oc} and efficiency.

With this composition-graded $(Cu_{1-x}Ag_x)_2ZnSn(S,Se)_4$ alloy as the absorber layer, it is not necessary to dope the near-interface region with high Ag composition to highly n-type or form a buried p–n junction inside the absorber layer between the regions with high Cu composition (p-type) and high Ag composition (n-type). If the near-interface region is intrinsic or weakly n-type (with the Fermi level near the middle of band gap), a p–n junction will be formed between the $(Cu_{1-x}Ag_x)_2ZnSn(S,Se)_4$ absorber layer and n-type CdS, and a large band bending will be produced inside the absorber layer

© 2015 WILEY-VCH Verlag GmbH & Co. KGaA, Weinheim

(with the Fermi level shifted up to close to CBM in the near-interface region, as shown in Figure 1c), so a large V_{oc} can still be achieved.

Since Ag is an expensive element, we should point out that there may be other elements that can also be alloyed into $Cu_2ZnSn(S,Se)_4$ and have similar function to the composition-graded $(Cu_{1-x}Ag_x)_2ZnSn(S,Se)_4$ alloy, then the cost can be reduced. Our current study may inspire the further theoretical and experimental study to find alternative cheap elements to replace Ag.

3. Conclusions

We show that the valence band edge energy has important influence on the formation of the acceptor defects including the I_{II} antisites in the Cu- and Ag-based I_2–II–IV–VI_4 quaternary semiconductors. Since the valence band edges of Cu_2ZnSnS_4 and Cu_2CdSnS_4 are high, the Cu_{Zn} and Cu_{Cd} antisites and the related defect complexes have high equilibrium concentrations, contributing to the high intrinsic p-type conductivity but also to the limited V_{oc} of the solar cells based on these systems, as have been experimentally observed. Since the valence band edge as well as the conduction band edge of Ag_2ZnSnS_4 are much lower than those of Cu_2ZnSnS_4, the formation energy of the acceptor defect Ag_{Zn} becomes higher than those of three donor defects (Zn_{Ag}, Sn_{Zn}, and V_S), which makes Ag_2ZnSnS_4 n-type although with low electron carrier concentration. Similar disparity in the defect properties and electrical conductivity are expected to exist also in other Cu- and Ag-based quaternary, ternary, and binary chalcogenide semiconductors, which are supported by the available experiments. Our study reveals an important disparity between the defect properties of Cu- and Ag-based I_2–II–IV–VI_4 semiconductors. Based on this disparity, we propose a strategy to overcome the V_{oc} bottleneck and increase the efficiency of the kesterite solar cells through forming a composition-graded $(Cu_{1-x}Ag_x)_2ZnSn(S,Se)_4$ alloy absorber.

4. Experimental Section

To predict what kinds of defects are dominant in Cu_2CdSnS_4 and Ag_2ZnSnS_4, we calculated the formation energy ΔH_f of a series of possible point defects

$$\Delta H_f(\alpha,q) = E(\alpha,q) - E(\text{host}) + \sum n_i(E_i + \mu_i) + q[\varepsilon_{VBM}(\text{host}) + E_F] \quad (1)$$

where α represents the defect and q is its charge state. As Equation (1) shows, ΔH_f is a function of the element chemical potential $E_i + \mu_i$ (describing the richness or partial pressure of elements in the synthesis atmosphere), and also a function of the Fermi level $\varepsilon_{VBM}(\text{host}) + E_F$ when it is charged (q is not zero). In the element chemical potential $E_i + \mu_i$, E_i is the reference and set to the total energy of the pure phase of the element i, e.g., face-centered-cubic Cu and Ag, hexagonal-close-packed Cd crystals, α-Sn, and α-S (S_8). $\mu_i = 0$ represents the limit where the element is so rich that the pure elemental phase will start to form. Since the quaternary semiconductor can be synthesized only in a certain atmosphere, μ_i of the component elements is limited in a range, which are given in Figure S1 (Supporting Information). The Fermi level is referenced to the energy level of valence band maximum (VBM) of the host $\varepsilon_{VBM}(\text{host})$, so $E_F = 0$ means that the Fermi level is at the VBM level, and $E_F = E_g$ means that the Fermi level is at the conduction band minimum (CBM).

The formation energy of point defects can be calculated using a supercell model in which one defect α is placed at the center of the supercell.[92] $E(\text{host})$ is the total energy of the host supercell free of defects, and $E(\alpha,q)$ is that of the defect-containing supercell. n_i is the number of atoms removed from the supercell to the external reservoir when the defect is formed, e.g., $n_i = +1$ (–1) if one atom is removed from (added to) the supercell. For a defect α, when its formation energy for two different charge states $q1$ and $q2$ are equal at a certain Fermi level, we define that Fermi level as its transition energy level $\varepsilon(\alpha, q1/q2)$. Therefore the transition energy levels can be derived when the formation energies of defects with different charge states are calculated. More details about the defect calculation models are given in refs. [14,15].

The total energy and electronic eigenvalues in Equation (1) are calculated using density function theory methods as implemented in the Vienna Ab-initio Simulation Package (VASP).[93] The generalized gradient approximation (GGA) to the exchange correlation functional is used as formulated by Perdew–Burke–Ernzerhof (PBE).[94] The GGA calculations usually overestimate the VBM level and underestimate the CBM level (thus underestimate the band gap), which causes the calculated formation energies of the acceptor and donor defect also underestimated, so a band edge correction is needed, as discussed in detail by Lany and Zunger.[95] In the current study, both the VBM overestimation and the CBM underestimation (Δ_{VBM} = 0.50 eV, Δ_{CBM} = 0.88 eV for Cu_2CdSnS_4, and Δ_{VBM} = 1.17 eV, Δ_{CBM} = 0.40 eV for Ag_2ZnSnS_4, determined according to the PBE+U and G0W0 calculations) are corrected through adding Δ_{VBM} (Δ_{CBM}) to the calculated formation energy of acceptor (donor) defects, following the same procedure as that used in the study of $CuGaSe_2$ and $CuInSe_2$.[34] After the correction, the calculated formation energies[15] are consistent with those from the hybrid functional calculations[16] for the Cu_2ZnSnS_4 defects. The formation energies of the dominant acceptor and donor defects (Cu_{Cd} and Cd_{Cu} in Cu_2CdSnS_4, and Ag_{Zn} and Zn_{Ag} in Ag_2ZnSnS_4) which determine the p-type or n-type conductivity are also calculated using the hybrid functional (HSE06). As shown in the supporting information, the results are close to those from the PBE calculation (after the band edge correction), so the conclusion of our current study is not influenced by the specific functionals that we used. For defects with deep levels (V_{Sn}, Cu_{Sn}, Sn_{Cd}, Sn_{Cu}, V_S, Cd_i, Ag_{Sn}, Sn_{Ag}, Sn_{Zn}), the GGA calculation tends to predict shallower transition energy levels, so we adapted a simple correction scheme through adding the dispersion difference between valence (conduction) band and acceptor (donor) defect band, which was found to give results more consistent with those from the hybrid functional calculations for deep level defects in Cu_2ZnSnS_4.[15,16]

The projector augmented-wave pseudopotentials[96] and an energy cutoff of 300 eV were used in all cases. A $2\times2\times2$ k-point mesh is used for the Brillouin zone integration of the 64-atom supercell. Test calculations showed that the results are well converged, i.e., the error is less than 0.03 eV with respect to the energy cutoff and the k-point mesh (test results with energy cutoff up to 500 eV and k-point mesh up to $4\times4\times4$ are shown in the Supporting Information) and the error is 0.1 eV with respect to the supercell size according to both test calculations by us with supercells as large as 512 atoms and by Han *et al* with supercells as large as 1728 atoms.[16] It should be noted that no correction is performed for the Coulomb interaction error of charged defects, so a larger error (0.1–0.2 eV) is possible for multivalent point defects, which is tolerable for the qualitative analysis in the present study.

Acknowledgements

The work at Fudan was supported by the Special Funds for Major State Basic Research, National Natural Science Foundation of China (NSFC), International collaboration project, Program for Professor of Special Appointment (Eastern Scholar), and Fok Ying Tung Education

© 2015 WILEY-VCH Verlag GmbH & Co. KGaA, Weinheim

Foundation. S.C. is supported by NSFC under Grant No. 91233121 and Shanghai Rising-Star Program (14QA1401500). The work at Bath is supported by the Royal Society and the EPSRC (Grant nos. EP/K016288/1 and EP/L017792/1). The work at NREL was funded by the U.S. Department of Energy (DOE), under Contract No. DE-AC36-08GO28308.

Received: June 3, 2015
Revised: August 30, 2015
Published online: October 19, 2015

[1] M. A. Green, K. Emery, Y. Hishikawa, W. Warta, E. D. Dunlop, *Prog. Photovoltaics* **2015**, *23*, 1.
[2] C. Wang, S. Chen, J.-H. Yang, L. Lang, H.-J. Xiang, X.-G. Gong, A. Walsh, S.-H. Wei, *Chem. Mater.* **2014**, *26*, 3411.
[3] C. H. L. Goodman, *J. Phys. Chem. Solids* **1958**, *6*, 305.
[4] F.-J. Fan, L. Wu, S.-H. Yu, *Energy Environ. Sci.* **2014**, *7*, 190.
[5] S. Chen, X. Gong, A. Walsh, S.-H. Wei, *Phys. Rev. B* **2009**, *79*, 165211.
[6] G. M. Ford, Q. Guo, R. Agrawal, H. W. Hillhouse, *Chem. Mater.* **2011**, *23*, 2626.
[7] S. Levcenco, D. Dumcenco, Y. Huang, E. Arushanov, V. Tezlevan, K. Tiong, C. Du, *J. Appl. Phys.* **2010**, *108*, 073508.
[8] I. Repins, C. Beall, N. Vora, C. DeHart, D. Kuciauskas, P. Dippo, B. To, J. Mann, W.-C. Hsu, A. Goodrich, R. Noufi, *Sol. Energy Mater. Sol. Cells* **2012**, *101*, 154.
[9] W. Wang, M. T. Winkler, O. Gunawan, T. Gokmen, T. K. Todorov, Y. Zhu, D. B. Mitzi, *Adv. Energy Mater.* **2014**, *4*, 1301465.
[10] F. Liu, K. Sun, W. Li, C. Yan, H. Cui, L. Jiang, X. Hao, M. A. Green, *Appl. Phys. Lett.* **2014**, *104*, 051105.
[11] H. Katagiri, K. Saitoh, T. Washio, H. Shinohara, T. Kurumadani, S. Miyajima, *Sol. Energy Mater. Sol. Cells* **2001**, *65*, 141.
[12] B. Shin, Y. Zhu, N. A. Bojarczuk, S. J. Chey, S. Guha, *Appl. Phys. Lett.* **2012**, *101*, 053903.
[13] H. Zhou, W.-C. Hsu, H.-S. Duan, B. Bob, W. Yang, T.-B. Song, C.-J. Hsu, Y. Yang, *Energy Environ. Sci.* **2013**, *6*, 2822.
[14] S. Chen, J.-H. Yang, X. Gong, A. Walsh, S.-H. Wei, *Phys. Rev. B* **2010**, *81*, 245204.
[15] S. Chen, A. Walsh, X.-G. Gong, S.-H. Wei, *Adv. Mater.* **2013**, *25*, 1522.
[16] D. Han, Y. Y. Sun, J. Bang, Y. Y. Zhang, H. B. Sun, X. B. Li, S. B. Zhang, *Phys. Rev. B* **2013**, *87*, 155206.
[17] K. Biswas, S. Lany, A. Zunger, *Appl. Phys. Lett.* **2010**, *96*, 201902.
[18] M. Grossberg, J. Krustok, J. Raudoja, T. Raadik, *Appl. Phys. Lett.* **2012**, *101*, 102102.
[19] S. Chen, X. Gong, A. Walsh, S.-H. Wei, *Appl. Phys. Lett.* **2010**, *96*, 021902.
[20] S. Levcenko, V. E. Tezlevan, E. Arushanov, S. Schorr, T. Unold, *Phys. Rev. B* **2012**, *86*, 045206.
[21] N. Nakayama, K. Ito, *Appl. Surf. Sci.* **1996**, *92*, 171.
[22] J. J. Scragg, P. J. Dale, L. M. Peter, G. Zoppi, I. Forbes, *Phys. Status Solidi B* **2008**, *245*, 1772.
[23] K. Ramasamy, M. A. Malik, P. O'Brien, *Chem. Commun.* **2012**, *48*, 5703.
[24] M. Suryawanshi, G. Agawane, S. Bhosale, S. Shin, P. Patil, J. Kim, A. Moholkar, *Mater. Sci. Technol.* **2013**, *28*, 98.
[25] A. Moholkar, S. Shinde, G. Agawane, S. Jo, K. Rajpure, P. Patil, C. Bhosale, J. Kim, *J. Alloys Compd.* **2012**, *544*, 145.
[26] M. Bär, B.-A. Schubert, B. Marsen, R. G. Wilks, S. Pookpanratana, M. Blum, S. Krause, T. Unold, W. Yang, L. Weinhardt, C. Heske, H.-W. Schock, *Appl. Phys. Lett.* **2011**, *99*, 222105.
[27] P. Würfel, in *Physics of Solar Cells*, Wiley-VCH, Weinheim, Germany **2007**, Ch. 6.
[28] A. Chirilă, S. Buecheler, F. Pianezzi, P. Bloesch, C. Gretener, A. R. Uhl, C. Fella, L. Kranz, J. Perrenoud, S. Seyrling, R. Verma, S. Nishiwaki, Y. E. Romanyuk, G. Bilger, A. N. Tiwari, *Nat. Mater.* **2011**, *10*, 857.
[29] U. Rau, H. W. Schock, *Appl. Phys. A* **1999**, *69*, 131.
[30] J. Kim, H. Hiroi, T. K. Todorov, O. Gunawan, M. Kuwahara, T. Gokmen, D. Nair, M. Hopstaken, B. Shin, Y. S. Lee, W. Wang, H. Sugimoto, D. B. Mitzi, *Adv. Mater.* **2014**, *26*, 7427.
[31] M. Graetzel, R. A. J. Janssen, D. B. Mitzi, E. H. Sargent, *Nature* **2012**, *488*, 304.
[32] R. Klenk, *Thin Solid Films* **2001**, *387*, 135.
[33] D. Liao, A. Rockett, *J. Appl. Phys.* **2003**, *93*, 9380.
[34] C. Persson, Y. J. Zhao, S. Lany, A. Zunger, *Phys. Rev. B* **2005**, *72*, 035211.
[35] F. Pianezzi, P. Reinhard, A. Chirila, B. Bissig, S. Nishiwaki, S. Buecheler, A. N. Tiwari, *Phys. Chem. Chem. Phys.* **2014**, *16*, 8843.
[36] J. P. Leitão, N. M. Santos, P. A. Fernandes, P. M. P. Salomé, A. F. da Cunha, J. C. González, G. M. Ribeiro, F. M. Matinaga, *Phys. Rev. B* **2011**, *84*, 024120.
[37] T. Gokmen, O. Gunawan, T. K. Todorov, D. B. Mitzi, *Appl. Phys. Lett.* **2013**, *103*, 103506.
[38] T. Gershon, B. Shin, N. Bojarczuk, T. Gokmen, S. Lu, S. Guha, *J. Appl. Phys.* **2013**, *114*, 154905.
[39] M. J. Romero, H. Du, G. Teeter, Y. Yan, M. M. Al-Jassim, *Phys. Rev. B* **2011**, *84*, 165324.
[40] M. Grossberg, J. Krustok, J. Raudoja, K. Timmo, M. Altosaar, T. Raadik, *Thin Solid Films* **2011**, *519*, 7403.
[41] B. G. Mendis, M. D. Shannon, M. C. J. Goodman, J. D. Major, A. A. Taylor, D. P. Halliday, K. Durose, *J. Phys.: Conf. Ser.* **2013**, *471*, 012014.
[42] J. P. Teixeira, R. A. Sousa, M. G. Sousa, A. F. da Cunha, P. A. Fernandes, P. M. P. Salomé, J. C. González, J. P. Leitão, *Appl. Phys. Lett.* **2014**, *105*, 163901.
[43] L. Yin, G. Cheng, Y. Feng, Z. Li, C. Yang, X. Xiao, *RSC Adv.* **2015**, *5*, 40369.
[44] M. E. Erkan, V. Chawla, I. Repins, M. A. Scarpulla, *Sol. Energy Mater. Sol. Cells* **2015**, *136*, 78.
[45] T. Gershon, Y. S. Lee, R. Mankad, O. Gunawan, T. Gokmen, D. Bishop, B. McCandless, S. Guha, *Appl. Phys. Lett.* **2015**, *106*, 123905.
[46] O. Gunawan, T. Gokmen, B. S. Shin, S. Guha, in *38th IEEE Photovoltaic Specialists Conf.*, IEEE, Austin, TX, USA **2012**, 003001.
[47] S. M. Pawar, B. S. Pawar, K. V. Gurav, D. W. Bae, S. H. Kwon, S. S. Kolekar, J. H. Kim, *Jpn. J. Appl. Phys.* **2012**, *51*, 10NC27.
[48] H. Katagiri, K. Jimbo, W. S. Maw, K. Oishi, M. Yamazaki, H. Araki, A. Takeuchi, *Thin Solid Films* **2009**, *517*, 2455.
[49] T. K. Todorov, K. B. Reuter, D. B. Mitzi, *Adv. Mater.* **2010**, *22*, E156.
[50] K. Wang, O. Gunawan, T. Todorov, B. Shin, S. J. Chey, N. A. Bojarczuk, D. Mitzi, S. Guha, *Appl. Phys. Lett.* **2010**, *97*, 143508.
[51] B. Shin, O. Gunawan, Y. Zhu, N. A. Bojarczuk, S. J. Chey, S. Guha, *Prog. Photovoltaics* **2013**, *21*, 72.
[52] A. D. Collord, H. W. Hillhouse, *Chem. Mater.* **2015**, *27*, 1855.
[53] W. Li, J. Chen, C. Yan, X. Hao, *J. Alloys Compd.* **2015**, *632*, 178.
[54] T. Washio, H. Nozaki, T. Fukano, T. Motohiro, K. Jimbo, H. Katagiri, *J. Appl. Phys.* **2011**, *110*, 074511.
[55] M. Courel, O. Vigil-Galán, D. Jiménez-Olarte, M. Espíndola-Rodríguez, E. Saucedo, *J. Appl. Phys.* **2014**, *116*, 134503.
[56] Y. Zhao, W. Tao, J. Liu, A. Wei, *Mater. Lett.* **2015**, *148*, 63.
[57] C. J. Hages, N. J. Carter, R. Agrawal, T. Unold, *J. Appl. Phys.* **2014**, *115*, 234504.
[58] B. G. Mendis, M. C. Goodman, J. D. Major, A. A. Taylor, K. Durose, D. P. Halliday, *J. Appl. Phys.* **2012**, *112*, 124508.
[59] J. J. Scragg, T. Ericson, T. Kubart, M. Edoff, C. Platzer-Björkman, *Chem. Mater.* **2011**, *23*, 4625.
[60] P. Bras, J. Sterner, C. Platzer-Björkman, *Thin Solid Films* **2015**, *582*, 233.

© 2015 WILEY-VCH Verlag GmbH & Co. KGaA, Weinheim

[61] L. Y. Yeh, K. W. Cheng, *Thin Solid Films* **2014**, *558*, 289.
[62] T. Sasamura, T. Osaki, T. Kameyama, T. Shibayama, A. Kudo, S. Kuwabata, T. Torimoto, *Chem. Lett.* **2012**, *41*, 1009.
[63] K. Ito, T. Nakazawa, *Jpn. J. Appl. Phys., Part 1* **1988**, *27*, 2094.
[64] W. G. Zhao, G. Wang, Q. W. Tian, L. J. Huang, S. Gao, D. C. Pan, *Sol. Energy Mater. Sol. Cells* **2015**, *133*, 15.
[65] S. Wagner, P. M. Bridenbaugh, *J. Cryst. Growth* **1977**, *39*, 151.
[66] Z. Su, J. M. R. Tan, X. Li, X. Zeng, S. K. Batabyal, L. H. Wong, *Adv. Energy Mater.* **2015**, DOI: 10.1002/aenm.201500682.
[67] S. B. Zhang, S.-H. Wei, A. Zunger, H. Katayama-Yoshida, *Phys. Rev. B* **1998**, *57*, 9642.
[68] J. Pohl, K. Albe, *Phys. Rev. B* **2013**, *87*, 245203.
[69] K. Timmo, M. Kauk-Kuusik, M. Altosaar, J. Raudoja, M. Pilvet, T. Raadik, T. Varema, I. Leinemann, in *Proc. 28th European Photovoltaic Solar Energy Conf. and Exhibition* (Eds: A. Mine, A. Jager-Waldau, P. Helm), EU PVSEC, Paris, France **2013**, 2385.
[70] I. Tsuji, Y. Shimodaira, H. Kato, H. Kobayashi, A. Kudo, *Chem. Mater.* **2010**, *22*, 1402.
[71] K. Li, B. Chai, T. Y. Peng, J. Mao, L. Zan, *RSC Adv.* **2013**, *3*, 253.
[72] K. Zhang, L. Guo, *Catal. Sci. Technol.* **2013**, *3*, 1672.
[73] K. Iwashina, A. Iwase, Y. H. Ng, R. Amal, A. Kudo, *J. Am. Chem. Soc.* **2014**, *137*, 604.
[74] S.-H. Wei, A. Zunger, *J. Appl. Phys.* **1995**, *78*, 3846.
[75] Y. Yan, S.-H. Wei, *Phys. Status Solidi B* **2008**, *245*, 641.
[76] S. B. Zhang, S.-H. Wei, A. Zunger, *J. Appl. Phys.* **1998**, *83*, 3192.
[77] Y. F. Yan, J. B. Li, S.-H. Wei, M. M. Al-Jassim, *Phys. Rev. Lett.* **2007**, *98*, 135506.
[78] S. Chen, X. Gong, A. Walsh, S.-H. Wei, *Appl. Phys. Lett.* **2009**, *94*, 041903.
[79] J. Paier, R. Asahi, A. Nagoya, G. Kresse, *Phys. Rev. B* **2009**, *79*, 115126.
[80] J. Jaffe, A. Zunger, *Phys. Rev. B* **1983**, *28*, 5822.
[81] J. Jang, K. Cho, S. H. Lee, S. Kim, *Mater. Lett.* **2008**, *62*, 1438.
[82] B. Tell, J. Shay, H. Kasper, *J. Appl. Phys.* **1972**, *43*, 2469.
[83] P. P. Ramesh, O. M. Hussain, S. Uthanna, B. S. Naidu, P. J. Reddy, *Mater. Lett.* **1998**, *34*, 217.
[84] H. P. Geserich, W. Suppanz, *Phys. Status Solidi B* **1969**, *35*, 381.
[85] S. S. Dhumure, C. D. Lokhande, *Thin Solid Films* **1994**, *240*, 1.
[86] Y. Ueno, Y. Hattori, M. Ito, T. Sugiura, H. Minoura, *Sol. Energy Mater. Sol. Cells* **1992**, *26*, 229.
[87] H. M. Pathan, P. V. Salunkhe, B. R. Sankapal, C. D. Lokhande, *Mater. Chem. Phys.* **2001**, *72*, 105.
[88] K. Hattori, K. Akamatsu, N. Kamegashira, *J. Appl. Phys.* **1992**, *71*, 3414.
[89] M. Ferhat, J. Nagao, *J. Appl. Phys.* **2000**, *88*, 813.
[90] K. Wei, G. S. Nolas, *ACS Appl. Mater. Interfaces* **2015**, *7*, 9752.
[91] Y. S. Lee, T. Gershon, O. Gunawan, T. K. Todorov, T. Gokmen, Y. Virgus, S. Guha, *Adv. Energy Mater.* **2015**, *5*, 1401372.
[92] S.-H. Wei, *Comput. Mater. Sci.* **2004**, *30*, 337.
[93] G. Kresse, J. Furthmuller, *Phys. Rev. B* **1996**, *54*, 11169.
[94] J. P. Perdew, K. Burke, M. Ernzerhof, *Phys. Rev. Lett.* **1996**, *77*, 3865.
[95] S. Lany, A. Zunger, *Phys. Rev. B* **2008**, *78*, 235104.
[96] G. Kresse, D. Joubert, *Phys. Rev. B* **1999**, *59*, 1758.

© 2015 WILEY-VCH Verlag GmbH & Co. KGaA, Weinheim